PHYSICAL REVIEW A VOLUME 15, NUMBER 3 MARCH 1977

Effect of chemical environment on the intensities of $K\alpha$ x-ray satellites produced in heavy-ion collisions*

R. L. Watson, A. K. Leeper, B. I. Sonobe, T. Chiao, and F. E. Jenson
Cyclotron Institute and Department of Chemistry, Texas A&M University, College Station, Texas 77843
(Received 29 July 1976)

High-resolution measurements of ion-excited $K\alpha$ x-ray spectra have been performed for a variety of Al, Si, S, and Cl compounds. An examination of the $K\alpha$ satellite intensity distribution revealed significant variations from one compound to another. This effect has been attributed to alteration of the K and/or L vacancy transfer rates due to the influence of chemical environment. The systematic trend displayed by the data tends to suggest that interatomic processes are important in the deexcitation of these highly ionized systems.

I. INTRODUCTION

Recent studies of inner-shell ionization resulting from ion-atom collisions have led to the discovery of a wide variety of interesting new phenomena.[1] Much of this effort has been directed toward delineating the various mechanisms by which inner-shell vacancies are produced during the collision process. A great deal of evidence has now accumulated which indicates that at ion velocities much less than the velocities of the inner-shell electrons, vacancies are produced primarily by electron promotion via level crossings while at very high ion velocities the principal mechanism for vacancy production is that of Coulomb excitation. A third mechanism, consisting of electron exchange from inner shells of target atoms to bound states of projectiles, is also of importance at low to intermediate ion velocities.

One of the most striking differences between inner-shell vacancy production by electron bombardment or by photoabsorption and that resulting from heavy-ion bombardment at intermediate velocities (around 1 MeV/amu), is the high degree of multiple ionization produced by the latter. Early studies by Burch and Richard,[2] for example, indicated that when a K-shell electron in a Ca atom is ionized by a 15-MeV oxygen ion, on the average three L-shell electrons and three to five M-shell electrons are removed in the same collision. Of particular interest with regard to the present work are the results of Knudson *et al.*[3] and Burch *et al.*[4] These investigators first demonstrated that the spectra of $K\alpha$ x-rays produced by heavy-ion bombardment (Ne and O) of intermediate to low-Z elements (Al and Fe) can be resolved into a series of satellite peaks, each of which is associated with $K\alpha$ x-ray emission in the presence of a specific number of L-shell vacancies. This discovery pointed toward the possibility of determining ionization cross sections for specific states of ionization produced in the collision process, thereby providing a means of testing in considerable detail various theories of multiple ionization. Unfortunately the problem of relating x-ray satellite intensities to vacancy production cross sections is complicated, not only because the x-ray emission probability is different for each vacancy configuration, but also because of the possible occurrence of various rearrangement processes prior to x-ray emission.[5,6] In fact if the probabilities for rearrangement processes are significant, they must be included in the definition of the fluorescence yield. While several fluorescence yield calculations for single K- plus multiple L-vacancy configurations have appeared in the literature,[7,8] none of them have taken L-vacancy transfer processes into account.

Several investigations of chemical effects on ion-excited x-ray spectra have been reported previously. Richard *et al.*[9] have examined the differences between the $K\alpha$ and $K\beta$ structure of Al and Al_2O_3 produced by protons and alpha particles, while Burkhalter *et al.*[10] have performed similar, but more detailed comparisons of the $K\alpha$ and $K\beta$ structure of Al, AlN, and Al_2O_3 using He and Ne ions. Additionally, McWherter *et al.*[11] have studied the $K\alpha$ and $K\beta$ structure of Si and SiO_2 produced by proton, He-, and O-ion bombardment. In all of these investigations, chemical shifts were observed for the various satellite peaks which were typically 1 eV or less for the $K\alpha$ lines and as much as 4 eV for the $K\beta$ lines. Fairly large and complicated changes in the structure of the various $K\beta$ satellites were also noted.

A recent examination of the relative intensities of $K\alpha$ x-ray satellites produced in a series of sulfur compounds by 2 MeV/amu oxygen and neon ions has revealed a dependence on chemical environment.[12] This effect was attributed to alteration of the vacancy distribution created at the time of collision by L vacancy transfer processes occurring prior to $K\alpha$ x-ray emission. We report here an extensive investigation of the effect of

chemical environment on $K\alpha$ x-ray satellites. Measurements of $K\alpha$ x-ray spectra have been performed on a number of solid compounds of Al, Si, S, and Cl using 32.4-MeV oxygen ions. Comparisons of $K\alpha$ satellite intensity distributions have also been made for several Si and S compounds using helium, carbon, neon, and argon ions.

II. EXPERIMENTAL METHODS

The detailed study of $K\alpha$ satellite spectra requires the use of a high-resolution crystal spectrometer because the energy differences between adjacent satellite peaks are quite small (typically ~15 eV). Furthermore, adaptation of a crystal spectrometer for in-beam use with a high-energy particle accelerator requires a rather compact, high-vacuum system with remote control of slit, crystal, and target adjustments. The system employed in the present study was a flat crystal Bragg spectrometer which has been described previously.[6] The Al and Si measurements were made with a pentaerythritol (PET) crystal and the S and Cl measurements were made with a NaCl crystal. The experimental energy resolution (full width at half maximum) of the $K\alpha_{1,2}$ peak was 3.7, 7.0, 5.5, and 11.2 eV for Al, Si, S, and Cl, respectively.

A schematic diagram of the experimental configuration is shown in Fig. 1. Beams of 5.4-MeV $^4He^{2+}$, 22.0-MeV $^{12}C^{3+}$, 32.4-MeV $^{16}O^{2+}$, 40.5-MeV $^{20}Ne^{3+}$, and 81.0-MeV $^{40}Ar^{5+}$ were extracted from the Texas A&M variable-energy cyclotron and focused on the target position by means of two sets of quadrupole magnets and a series of collimators. The diameter of the beam spot was typically 0.6 cm. The spectrometer was positioned at 90° with respect to the incident beam (45° with respect to the target). A set of entrance soller slits was used to limit the dispersion of the x rays which impinged on the Bragg crystal to approximately 0.5°. Detection of the reflected x rays was accomplished by means of a gas flow proportional counter (10% methane, 90% argon) having an aluminum coated (100 $\mu g/cm^2$) Mylar (530 $\mu g/cm^2$) window.

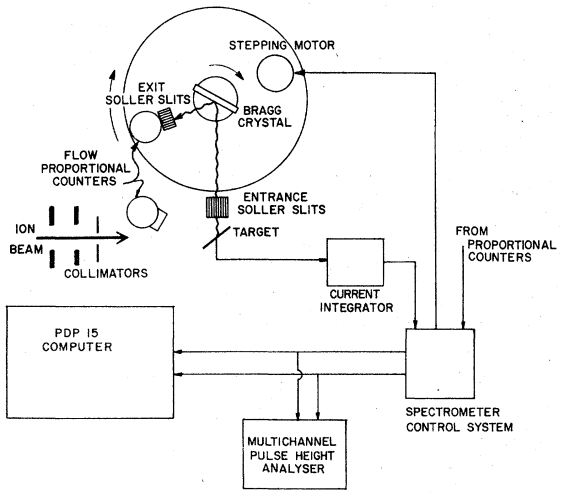

FIG. 1. Schematic diagram of the experimental configuration.

Automatic control of the spectrometer was provided by a specially designed control system.[6] Signals from the x-ray counter were sent to a single-channel analyzer where an energy window was set around the x rays of interest. The output signals from the single-channel analyzer then went to the spectrometer control system from which they were sent to a multichannel analyzer operated in the external-multiscale mode and to a PDP 15 computer. Beam monitor signals were obtained either by integrating the current generated in the target or by detecting x rays in another gas-flow proportional counter having a direct view of the target. The counting time at each spectrometer angle was determined by the number of monitor counts selected on thumb-wheel switches in the control unit. When the selected number of monitor counts had been collected, the system automatically stepped the spectrometer to the next counting position and advanced the analyzer and PDP 15 multiscalars. Utilization of the PDP 15 computer enabled on-line data analysis of a preceding spectrum while a new spectrum was accumulating.

Targets were prepared by compacting finely ground powders in a pellet press. The resulting 1.3-cm-diam by 0.3-cm-thick pellets were then attached to 2.3-mg/cm^2 Ni backings with a small amount of glue. In this way, it was possible to maintain a high degree of uniformity among all of the compounds investigated. A number of thin target measurements were also carried out and compared with the thick target results for Al, Al_2O_3, SiO, S_8, Na_2SO_4, Na_2S, NaCl, and KCl. Thicknesses of these targets ranged from 0.2 to 1.2 mg/cm^2. All of them were prepared by vacuum evaporation onto Ni backings except for the Al targets which were made from self-supporting Al foils and the Al_2O_3 targets which were made by electrolytic anodization. It was found to be necessary to cover the S_8 and $(NH_4)_2SO_4$ targets with 20-$\mu g/cm^2$ carbon foils in order to prevent evaporation of these substances during irradiation.

The beam levels were kept as low as possible in order to minimize target decomposition. Generally beam currents were of the order of 50 nA or less with the beam dispersed over a 0.6-cm-

diam region of the target. The time required to accumulate a single $K\alpha$ satellite spectrum ranged from as little as 3 min for Si to as much as 1 h for Na_2SO_4. As a further check against decomposition, at least three consecutive measurements with the same target were carried out in each run and the resulting spectra were carefully examined for a beam-dose dependence. In the case of highly volatile substances, such as S_8, evaporation effects were eliminated by using the total number of K x rays detected with a flow proportional counter having a direct view of the target (see Fig. 1) to generate the spectrometer monitor signals rather than using the current integrator method. Additional checks in which the intensity of the second $K\alpha$ satellite peak was monitored as a function of irradiation time were also performed.

III. ANALYSIS

For the present purpose of making detailed comparisons of $K\alpha$ x-ray satellite intensity distributions it is convenient to define a parameter which we shall refer to as the apparent average L-vacancy fraction, p_L.[13] Let f_n represent the fraction of the total $K\alpha$ x-ray yield contained in the nth satellite peak where n is the number of L-shell vacancies. Then the apparent average L-vacancy fraction is defined as

$$p_L \equiv \frac{\bar{n}}{N_L} = \frac{1}{N_L} \sum_n n f_n , \tag{1}$$

where N_L is the number of L-shell electrons in the ground-state atom. It is important to recognize that p_L as defined by Eq. (1) does not directly represent the average fraction of L-shell electrons which are missing at the time of $K\alpha$ x-ray emission since the fluorescence yields are different for the various L-vacancy configurations. We have merely chosen this as the parameter to be used in comparing $K\alpha$ x-ray satellite spectra because of its connection to the approximate relative satellite intensities through the binomial formula

$$f_n \approx \binom{N_L}{n} p_L^n (1-p_L)^{N_L - n} , \tag{2}$$

where $\binom{N_L}{n}$ is the binomial coefficient.[6,14]

The analysis procedure involved first carrying out a nonlinear least-squares fit to the $K\alpha$ satellite spectrum employing a Gaussian-plus-exponential-tail peak fitting function to extract the relative satellite intensities. An example of a typical fitted spectrum has been given previously.[6] The satellite intensities were then corrected for absorption in the target, for absorption in the proportional counter window, and for detection efficiency.

Because the x-ray absorption and projectile energy loss characteristics depend on the elemental composition of the target, care was taken to properly account for these differences. The considerations which entered into correcting for the use of thick targets are illustrated in Fig. 2. As a heavy ion penetrates the target, it loses energy and as a result the K-shell ionization cross section decreases with increasing penetration depth x (see σ/σ_0 curve in Fig. 2b). At the same time, the transmission probability of the emitted x rays also decreases (see I/I_0 curve in Fig. 2b). These two factors combine to determine a depth profile for x-ray detection which in turn determines the effective average energy of the ion beam in the target (see Fig. 2c–N/N_T is the fraction of the total *transmitted* x-ray yield produced up to depth x). In the case of 32.4-MeV oxygen ions incident on a thick SiO target, the average depth for x-ray de-

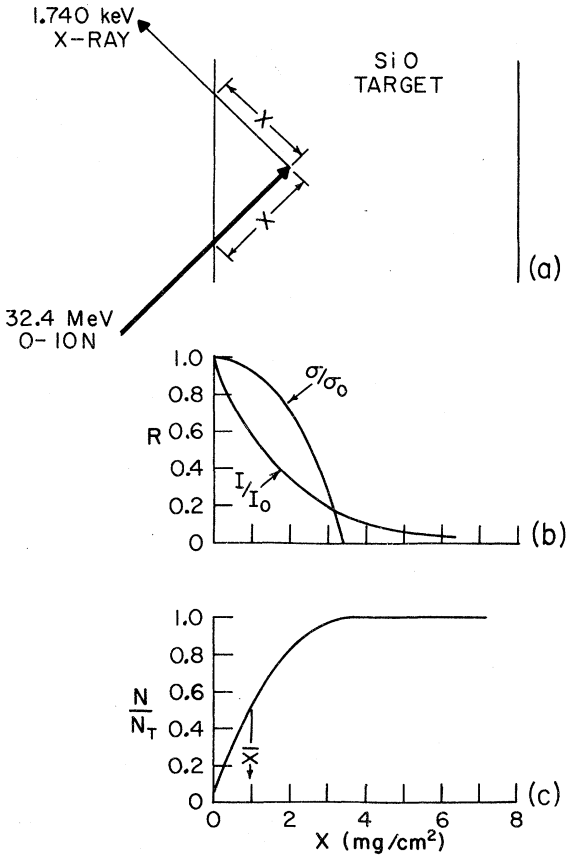

FIG. 2. An illustration of the effect of a thick (SiO) target on the production and detection of (Si) K x rays; (a) projectile and x-ray paths, (b) relative x-ray production (σ/σ_0) and transmission (I/I_0) curves as a function of depth, and (c) fraction of total transmitted x-ray yield produced up to depth x. ($\bar{x}$ is the average depth for x-ray production plus transmission.)

tection is calculated to be about 1 mg/cm^2 which translates into an average energy loss of 6 MeV.

Formally, the thick target corrections were calculated as follows: (a) Transmission correction. The rate per unit solid angle of x-ray production is

$$R_p = \frac{R_B f N_A \omega}{W_{\text{at.}}} \int_0^t \sigma(x)\, dx , \tag{3}$$

where R_B is the incident particle rate, ω, the fluorescence yield, f the weight fraction of the element of interest, N_A is Avogadro's number, $W_{\text{at.}}$ is the atomic weight of the element of interest, t is the target thickness in g/cm^2, and $\sigma(x)$ is the cross section for K-shell ionization at depth x, given by

$$\sigma(x) = \sigma_0 - \int_0^x \frac{d\sigma}{dE}\frac{dE}{dx}\, dx , \tag{4}$$

with σ_0 being the K-shell ionization cross section for the incident beam energy. The rate per unit solid angle at which x rays are transmitted out the front of the target as shown in Fig. 2(a) is

$$R_t = \frac{R_B f N_A \omega}{W_{\text{at.}}} \int_0^t \sigma(x) T(x)\, dx , \tag{5}$$

where $T(x) = e^{-ux}$, and u is the mass absorption coefficient.

The average x-ray transmission is then given by

$$\bar{T} = \frac{R_t}{R_p} = \frac{\int_0^t \sigma(x) T(x)\, dx}{\int_0^t \sigma(x)\, dx} . \tag{6}$$

Transmission corrections were calculated by numerical integration of Eq. (6) for each peak appearing in the $K\alpha$ x-ray spectrum. The binary encounter model results of Garcia[15] were used to obtain σ_0 and $d\sigma/dE$, and the dE/dx values were derived from the stopping-power tables of Northcliffe and Schilling.[16] Mass absorption coefficients were taken from Storm and Israel.[17] Further correction of the relative satellite intensities measured for AlSi (Al x rays), Al_2S_3 (Al x rays), and KCl (Cl x rays) were required to account for the enhancement of the $K\alpha_{1,2}$ peak due to photoionization by x rays from the higher-z components of these targets.[6]

(b) Projectile energy loss correction. Since the relative satellite intensities also depend on projectile energy, it was necessary to correct the measured p_L values for energy loss in the target. The average projectile energy for the *detection* of K x-rays was calculated from the relationship

$$\bar{E} = \frac{\int_0^t E(x)\sigma(x)T(x)\, dx}{\int_0^t \sigma(x)T(x)\, dx} , \tag{7}$$

where

$$E(x) = E_0 - \int_0^x \frac{dE}{dx}\, dx$$

in which E_0 is the incident beam energy. Using the results of detailed thin-target measurements of the variation of p_L with beam energy (which will be reported elsewhere[18]) and the average beam energy as calculated by Eq. (7), a correction was applied to each measured p_L value to get the p_L value corresponding to the *incident* beam energy. Further details of the calculation involved in (a) and (b) above may be found in Ref. 19.

Numerous comparisons of thick- and thin-target measurements were carried out for Al, Al_2O_3, SiO, S_8, Na_2SO_4, Na_2S, NaCl, and KCl in order to check the accuracy of the various corrections mentioned above. In all cases agreement between the corrected thick target and thin target results was within the experimental error. An example of the kind of agreement attained in these comparisons is shown in Fig. 3. The solid data points for SiO were measured using a 335 μg/cm^2 target while the open data points were measured with a thick pellet and are plotted at the calculated average thick-target energies. As can be seen, the thick-target data points agree well with the curve determined by the thin-target measurements. All of the data points for Si in Fig. 3 were measured with a thick target. Additional checks of the absorption corrections were performed by placing absorbers between the target and the entrance soller slits to the spectrometer.

IV. RESULTS

Examples of the effects of chemical environment on Si, S, and Cl $K\alpha$ x-ray spectra produced by 32.4-MeV oxygen-ion bombardment are shown in

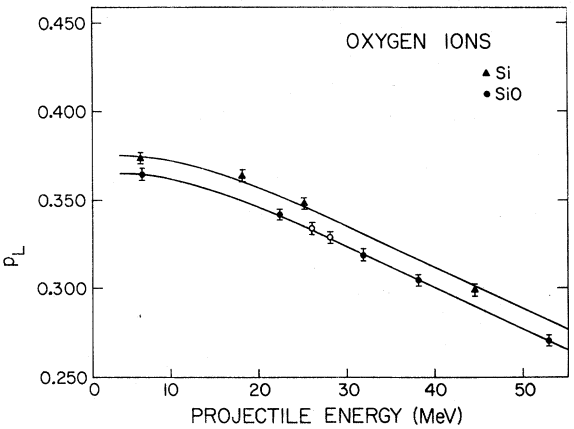

FIG. 3. Dependence of p_L for Si $K\alpha$ x rays on oxygen-ion energy. The solid data points for SiO are thin-target measurements, whereas the open data points are thick-target measurements employing 32.4-MeV oxygen ions. All of the data points for Si are thick target results.

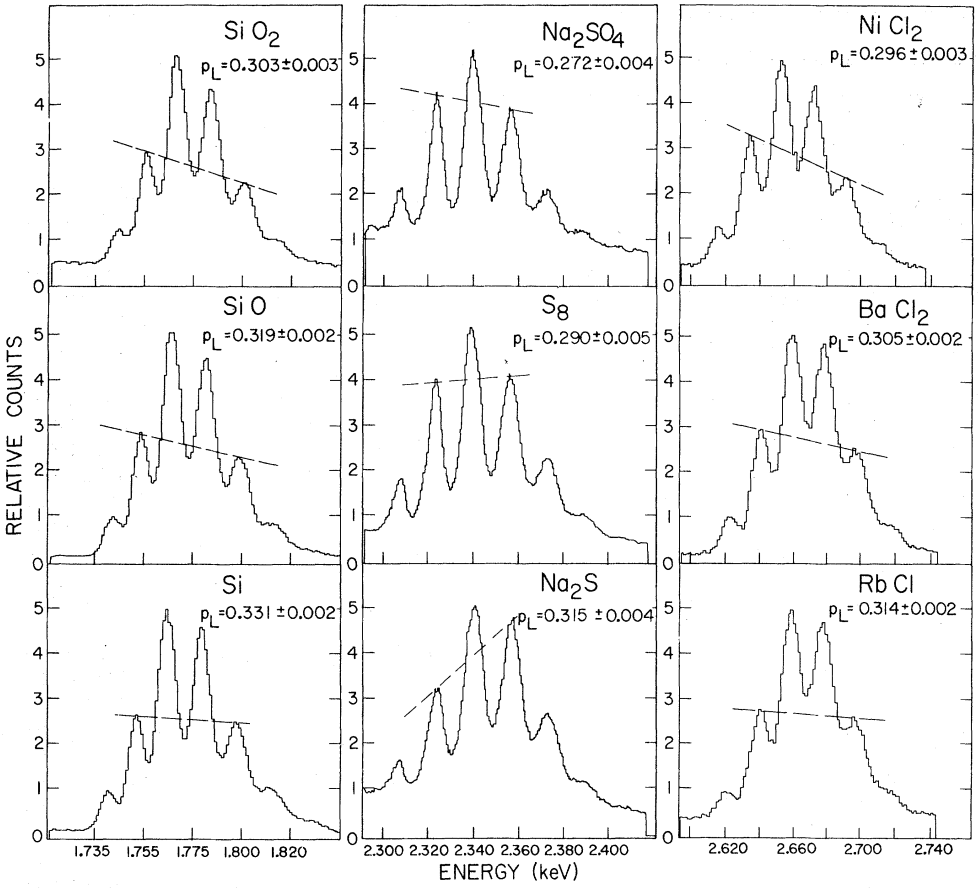

FIG. 4. Sample $K\alpha$ satellite spectra for several Si, S, and Cl compounds showing the variation of the relative satellite intensities with chemical environment. These spectra were all taken with 32.4-MeV oxygen ions.

Fig. 4. It is seen that the intensity distributions change markedly in going from the top spectra, where the satellite intensities are skewed toward the lower order satellites, to the bottom spectra, where they are skewed more toward the higher-order satellites. (The dashed lines in Fig. 4 are drawn to emphasize these changes.) Analysis of these spectra, including corrections for the average energy losses of the oxygen beam in the various targets, yields the apparent average L-vacancy fractions listed above each spectrum.

The measured $K\alpha$ x-ray relative intensities are listed in Table I for all of the compounds of Al, Si, S, and Cl investigated using 32.4-MeV oxygen ions. Also included in this table are the average thick-target beam energies and the p_L values before and after correction for projectile energy loss. The ranges of variation of the energy corrected p_L values for the four sets of compounds are compared in Fig. 5. Here it is seen that a large range of variation is observed for sulfur compounds while the range of variation for silicon compounds is about 30% less and the range of variation for chlorine compounds is almost 60% less. The p_L values for aluminum compounds vary less than do those for any of the other three sets of compounds.

Measurements were also carried out with a variety of other ions to assess the extent to which the $K\alpha$ satellite intensity effect depends on projectile atomic number. Shown in Fig. 6 are sulfur $K\alpha$ x-ray spectra produced by 40.5-MeV neon ions and 81.0-MeV argon ions incident on targets of Na_2S, S_8, and Na_2SO_4. It is apparent that the neon-ion-induced spectra exhibit essentially the same trend as was observed with oxygen ions. The spectra obtained with argon ions appear quite different from those obtained with neon ions in that the intensities of the $K\alpha_{1,2}$ peaks are considerably enhanced. This effect has been noted previously[6,20] and presumably indicates the presence of another mechanism for the creation of K-shell vacancies in collisions in which the projectile atomic number is somewhat larger than the target atomic number. Nevertheless, it is apparent that the satellite peak intensities change in much the same way in the argon-ion spectra as they do in the oxygen- and neon-ion spectra in going from Na_2S to Na_2SO_4.

The results of the measurements with He, C, Ne, and Ar ions are given in Table II. The p_L

TABLE I. Relative $K\alpha$ x-ray satellite intensities and p_L values for Al, Si, S, and Cl compounds using 32.4-MeV oxygen ions.

	f_n[a]										
Compound	$n=0$	$n=1$	$n=2$	$n=3$	$n=4$	$n=5$	$n=6$	NOM[b]	$\overline{E}$[c]	p_L[d]	p_L(corr)[e]
Aluminum											
Al	0.047	0.118	0.315	0.289	0.164	0.067		13	25.2	0.328	0.311 ±0.002
AlSi	0.063	0.112	0.314	0.280	0.166	0.067		6	25.6	0.325	0.309 ±0.002
Al_2S_3	0.051	0.129	0.329	0.291	0.150	0.051		6	26.8	0.315	0.302 ±0.002
Al_4C_3	0.046	0.125	0.338	0.291	0.154	0.045		5	25.5	0.315	0.299 ±0.004
AlB_2	0.043	0.120	0.319	0.298	0.160	0.060		3	24.9	0.324	0.307 ±0.002
AlN	0.051	0.122	0.335	0.291	0.152	0.048		8	26.1	0.317	0.302 ±0.002
Al_2O_3	0.053	0.136	0.326	0.292	0.141	0.053		4	26.8	0.317	0.304 ±0.002
Silicon											
AlSi	0.039	0.138	0.278	0.292	0.152	0.085	0.032	8	29.7	0.342	0.336 ±0.003
Si	0.038	0.131	0.270	0.285	0.153	0.091	0.033	31	25.2	0.348	0.331 ±0.002
SiO	0.039	0.144	0.295	0.292	0.138	0.072	0.020	14	26.1	0.334	0.319 ±0.002
SiB_6	0.034	0.139	0.287	0.295	0.149	0.078	0.018	5	24.6	0.337	0.319 ±0.003
SiC	0.038	0.143	0.295	0.292	0.143	0.068	0.022	4	25.2	0.331	0.314 ±0.002
SiO_2	0.040	0.180	0.306	0.299	0.133	0.061	0.010	6	26.5	0.317	0.303 ±0.003
Si_3N_4	0.042	0.153	0.302	0.294	0.136	0.066	0.017	7	25.7	0.322	0.306 ±0.003
Sulfur											
Na_2S	0.043	0.143	0.301	0.296	0.167	0.048	0.009	8	27.3	0.325	0.315 ±0.004
CdS	0.066	0.179	0.304	0.259	0.138	0.042	0.012	6	29.4	0.300	0.294 ±0.002
Al_2S_3	0.048	0.157	0.314	0.285	0.150	0.045		2	27.5	0.308	0.298 ±0.005
ZnS	0.049	0.180	0.307	0.274	0.148	0.039	0.005	7	29.0	0.301	0.294 ±0.003
S_8	0.054	0.176	0.308	0.267	0.141	0.047	0.011	18	25.3	0.304	0.290 ±0.005
FeS	0.051	0.179	0.305	0.265	0.140	0.046	0.012	3	28.5	0.303	0.295 ±0.002
Na_2SO_3	0.052	0.202	0.340	0.265	0.113	0.026	0.001	7	26.7	0.283	0.271 ±0.003
Na_2SO_4	0.053	0.207	0.342	0.257	0.108	0.030	0.006	13	26.6	0.284	0.272 ±0.004
$(NH_4)_2SO_4$	0.061	0.215	0.343	0.241	0.109	0.031		3	25.4	0.277	0.263 ±0.005
Chlorine											
RbCl	0.033	0.149	0.304	0.308	0.169	0.038		4	29.9	0.318	0.314 ±0.002
CsCl	0.039	0.153	0.306	0.299	0.163	0.040		7	29.1	0.314	0.306 ±0.002
KCl	0.063	0.137	0.287	0.299	0.170	0.044		18	25.5	0.320	0.304 ±0.003
NaCl	0.036	0.144	0.297	0.306	0.173	0.043		12	26.2	0.322	0.308 ±0.003
$BaCl_2$	0.042	0.157	0.300	0.298	0.162	0.041		5	29.0	0.313	0.305 ±0.002
$SrCl_2$	0.039	0.160	0.302	0.297	0.165	0.038		3	29.4	0.313	0.306 ±0.003
$CaCl_2$	0.051	0.148	0.297	0.296	0.167	0.042		7	25.6	0.313	0.297 ±0.004
NH_4Cl	0.043	0.146	0.293	0.301	0.173	0.044		7	25.2	0.320	0.303 ±0.002
$ZnCl_2$	0.046	0.169	0.302	0.287	0.156	0.039		4	29.2	0.307	0.300 ±0.002
$MnCl_2$	0.043	0.161	0.300	0.292	0.163	0.041		5	26.4	0.312	0.298 ±0.004
$BeCl_2$	0.045	0.155	0.288	0.293	0.173	0.045		4	25.1	0.316	0.299 ±0.004
LiCl	0.044	0.145	0.291	0.298	0.175	0.047		4	25.2	0.320	0.303 ±0.002
$MgCl_2$	0.040	0.152	0.296	0.295	0.171	0.045		4	26.4	0.317	0.303 ±0.002
$NiCl_2$	0.046	0.172	0.304	0.282	0.159	0.039		7	27.2	0.308	0.296 ±0.003

[a] Ratio of the nth satellite peak intensity to the sum of the intensities of all the $K\alpha$ peaks—corrected for absorption in the target and detector window, and for detector efficiency.

[b] Number of measurements from which f_n and p_L were derived.

[c] Calculated average beam energy (MeV) for the *detection* of $K\alpha$ x rays.

[d] p_L value determined directly from the f_n.

[e] p_L value corrected for projectile energy loss. The indicated errors are experimental root-mean-square deviations.

value listed for each argon-ion spectrum was obtained by an iterative procedure in which the relative intensity of the first x-ray peak (the $K\alpha_{1,2}$ peak) was replaced by the binomial intensity calculated from Eq. (2) using the p_L value from the preceding iteration. In this way p_L values which characterize only the satellite intensity distribution and are therefore unaffected by the $K\alpha_{1,2}$ intensity enhancement were obtained. As may be seen from the p_L values listed in Table II, the same kind of effect is observed with all of the projectiles down to and including carbon ions. The absence of an observable effect for helium ions with which only the first two satellite peaks are

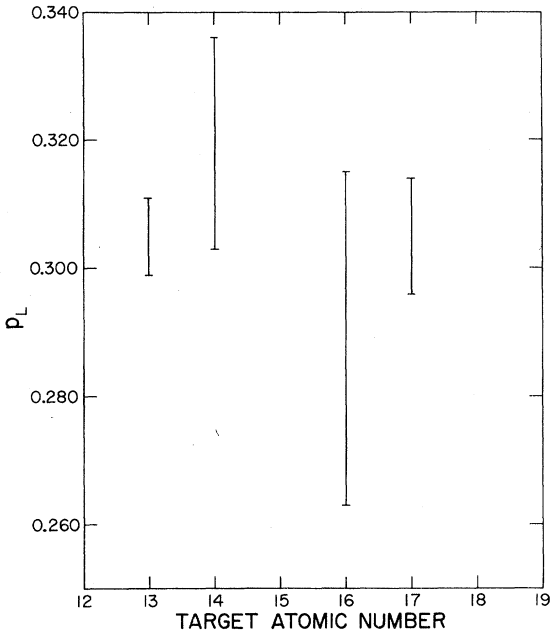

FIG. 5. Observed range of variation in p_L for the various sets of compounds examined using 32.4-MeV oxygen ions.

produced with significant intensities suggests that it is the higher-order satellites which are primarily responsible for the intensity variations.

V. DISCUSSION

In seeking to understand the cause of the observed $K\alpha$ x-ray satellite intensity variations, two possibilities must be considered. Either the effect is associated with the vacancy production process which occurs during the collision or it is associated with the deexcitation process which follows. It is conceivable that the chemical environment could influence the vacancy distribution produced in the collision to the extent that excitation to bound states and molecular orbital promotion are involved in the creation of L-shell vacancies; however at the beam energies employed in the present investigation, these processes are thought to be quite improbable. Recoil effects are also expected to be negligible as may be seen by referring to Table III in which calculated recoil energies for oxygen, neon, and argon ions incident on sulfur are listed. The bond distances in the sulfur compounds studied typically range

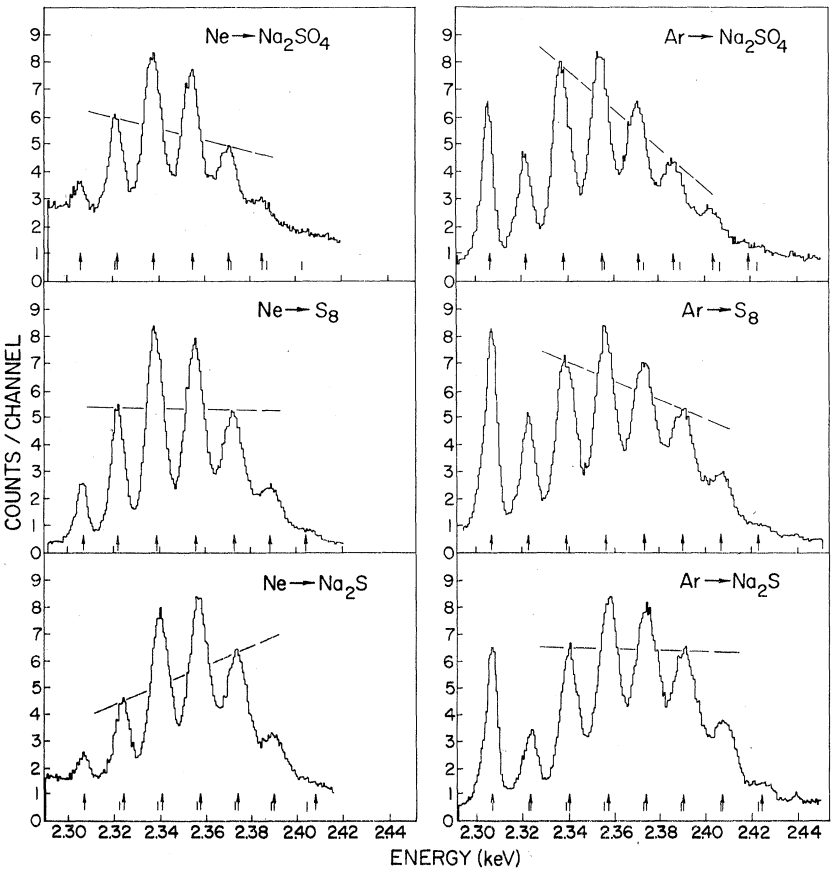

FIG. 6. $K\alpha$ x-ray spectra for 2-MeV/amu neon and argon ions incident on several sulfur compounds. The arrows indicate the peak centroids in each spectrum while the adjacent shorter lines in the Na_2SO_4 and Na_2S spectra show the locations of the peak centroids in the S_8 spectra.

TABLE II. Relative $K\alpha$ x-ray satellite intensities and p_L values for several Si and S compounds using He, C, Ne, and Ar ions.

Projectile and compound	f_n[a] $n=0$	$n=1$	$n=2$	$n=3$	$n=4$	$n=5$	$n=6$	$n=7$	NOM[b]	$\bar{E}$[c]	p_L[d]	p_L(corr)[e]
5.42-MeV He												
Si	0.524	0.384	0.093						3	4.46	0.071	0.058±0.002
SiO	0.529	0.382	0.089						3	4.60	0.070	0.060±0.002
SiO_2	0.545	0.370	0.085						3	4.65	0.068	0.060±0.002
22.0-MeV C												
Si	0.057	0.225	0.347	0.270	0.102				3	14.2	0.267	0.226±0.002
SiO	0.058	0.230	0.357	0.260	0.095				3	14.0	0.263	0.220±0.002
SiO_2	0.062	0.234	0.366	0.253	0.084				3	13.6	0.258	0.213±0.002
40.5-MeV Ne												
Na_2S	0.024	0.088	0.236	0.304	0.229	0.098	0.022		4	33.7	0.376	0.365±0.002
S_8	0.046	0.128	0.253	0.267	0.190	0.091	0.024		6	31.3	0.350	0.334±0.003
Na_2SO_4	0.034	0.137	0.291	0.287	0.168	0.066	0.017		4	33.0	0.336	0.323±0.005
81.0-MeV Ar												
Na_2S	0.100	0.056	0.138	0.204	0.219	0.175	0.090	0.018	4	66.7	0.469±0.002	
S_8	0.108	0.085	0.169	0.192	0.198	0.146	0.078	0.023	4	61.9	0.433±0.002	
Na_2SO_4	0.104	0.086	0.198	0.223	0.195	0.118	0.060	0.016	8	65.2	0.396±0.004	

[a] Ratio of the nth satellite peak intensity to the sum of the intensities of all the $K\alpha$ peaks—corrected for absorption in the target and detector window, and for detector efficiency.

[b] Number of measurements from which f_n and p_L were derived.

[c] Calculated average beam energy (MeV) for the *detection* of $K\alpha$ x rays.

[d] p_L value determined directly from the f_n. In the case of the Ar ion results an iterative procedure was used (see text) and data for energy loss corrections were not available.

[e] p_L value corrected for projectile energy loss. The indicated errors are experimental root-mean-square deviations.

from about 2 to 3 Å. The average distance a recoil travels within a K-hole lifetime (as given in Table III) is only a small fraction of a bond length. The fact that similar intensity variations are observed with a variety of different projectiles ranging from carbon to argon ions further supports the assumption that the cause of this effect is connected to the deexcitation process rather than to the excitation process.

A particular KL^n vacancy state, once formed, will eventually decay by one of the following ways: (a) K-vacancy transfer via a K x-ray transition, (b) K-vacancy transfer via a K Auger transition, or (c) L-vacancy transfer via an L Auger or L x-ray transition. We shall assume that multielectron transitions in which two or more vacancies are transferred simultaneously are sufficiently improbable that they may be neglected, although this may not be strictly true for the higher-order KL^n states. Let $f_{K\alpha}(n)$ be the probability for $K\alpha$ x-ray emission from vacancy state KL^n and similarly let $f_{K\beta}(n)$ be the probability for $K\beta$ x-ray emission, $f_{KA}(n)$ the probability for K Auger decay, and $f_L(n)$ the probability for L-vacancy transfer. Then it follows that

$$f_{K\alpha}(i)+f_{K\beta}(i)+f_{KA}(i)+f_L(i)=1\ . \tag{8}$$

The quantity $f_{K\alpha}(i)$ is by definition the $K\alpha$ fluorescence yield for configuration KL^i. The number of $K\alpha$ x rays originating from KL^i vacancy configurations $N^{\alpha}_{KL}(i)$ is related to the numbers of these and higher-order vacancy configurations produced in ion-atom collisions $N^{V}_{KL}(j)$ by the equation

$$N^{\alpha}_{KL}(i)=f_{K\alpha}(i)[N^{V}_{KL}(i)+f_L(i+1)N^{V}_{KL}(i+1) +f_L(i+1)f_L(i+2)N^{V}_{KL}(i+2)+\cdots]\ , \tag{9}$$

where i may be any integer from zero to N_L-1,

TABLE III. Calculated recoil energies and average recoil distances for various heavy ions incident on sulfur.

Projectile	Recoil energy[a] (eV)	Recoil distance[b] (Å)
27-MeV O	56	0.20
34-MeV Ne	87	0.25
67-MeV Ar	285	0.46

[a] Calculated using the distance of maximum K-electron density as given by Desclaux (Ref. 21) for the most probable impact parameter for K-shell ionization.

[b] Calculated using a mean K-hole lifetime of 1.11×10^{-15} sec.

or conversely

$$N^V_{KL}(i)=\frac{1}{f_{K\alpha}(i)}N^\alpha_{KL}(i)-\frac{f_L(i+1)}{f_{K\alpha}(i+1)}N^\alpha_{KL}(i+1)\ . \qquad (10)$$

[Eq. (10) can be shown to be true by substituting it into Eq. (9) for each $N^V_{KL}(j)$.]

It is obvious from Eq. (9) that if the $f_{K\alpha}$ and/or the f_L are sensitive to the chemical environment of the ionized atom, the $K\alpha$ satellite intensities will be directly affected. For the elements of interest here, L-vacancy transfer processes must involve the valence electrons and hence it is quite reasonable to expect these transition rates to be influenced by chemical bonding. Likewise, the fluorescence yields should also exhibit a dependence on chemical environment primarily caused by changes in the KLM and KMM Auger rates. These transitions are particularly important for the higher-order KL^n states in which the L electron populations are highly depleted.

In general, it is to be expected that the rates of K- and L-vacancy filling transitions will depend to a large extent upon the spatial overlap of the initial and final states. A relative measure of this overlap from one compound to another is provided by the effective density of those electrons which are involved in the transitions of interest. In the case of valence electrons these effective densities may be considerably altered by chemical bonding. An analysis of the trend displayed by the silicon and sulfur data in terms of effective valence electron density leads to an interesting conclusion regarding the general nature of the transitions involved in the $K\alpha$ satellite intensity variation effect. Referring back to Fig. 4 it is seen that p_L increases in going from Na_2SO_4 to Na_2S. This implies that $f_{K\alpha}$ and/or f_L are larger for Na_2SO_4 than for Na_2S. However, in Na_2SO_4 the formal oxidation state of sulfur is 6^+, signifying that a large fraction of the sulfur atom valence electron density has been transferred to the surrounding oxygen ligands, whereas in Na_2S the formal oxidation state of sulfur is 2^-, signifying that the sulfur-atom valence electron density has been increased by the transfer of electrons from the two neighboring sodium atoms. Hence it follows that transitions from the valence levels of sulfur atoms in Na_2S should be enhanced relative to transitions from the valence levels of sulfur atoms in Na_2SO_4, which is the exact opposite of what is indicated by the $K\alpha$ x-ray spectra. Similar arguments also apply to the set of compounds SiO_2, SiO, and Si.

The apparent contradiction outlined above leads us to conclude that transitions from the valence levels of neighboring atoms must contribute in a major way to K- and L-vacancy filling in multiply-ionized sulfur and silicon atoms. Such "interatomic" or "crossover" transitions were first postulated by Valasek[22] in 1938 and have since been the subject of numerous experimental and theoretical investigations. The role of interatomic transitions in the x-ray and Auger decay of ionized systems formed by photoabsorption or electron bombardment has recently been discussed by Åberg[23] and by Citrin.[24] Despite the great amount of interest in interatomic transitions, very little detailed information on their properties has yet evolved. In Fig. 7 several possible types of L-vacancy transfer transitions are illustrated schematically.

The satellite energy shifts shown in Fig. 6 provide further evidence of the involvement of electrons from surrounding atoms. It is observed that the higher-order satellites in Na_2SO_4 are shifted *down* in energy from the corresponding ones in S_8 while those in Na_2S are shifted *up* in energy. This implies that vacancies produced

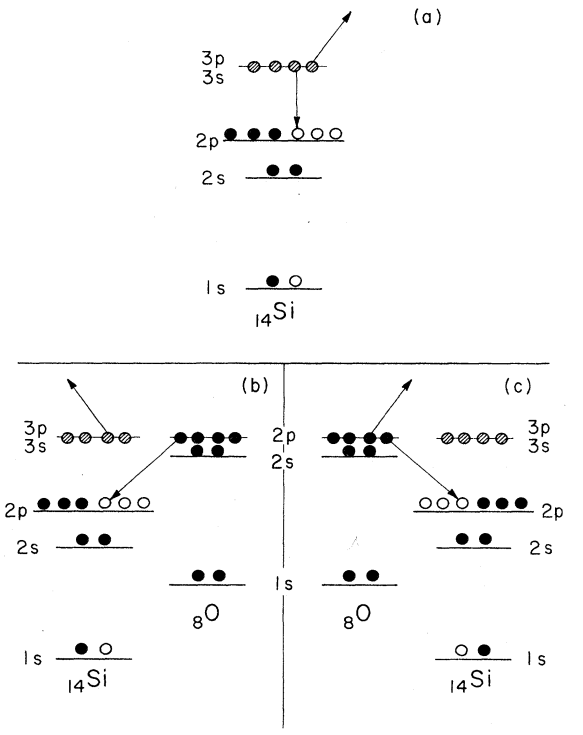

FIG. 7. Schematic illustration of several possible types of L vacancy transfer transitions for SiO: (a) intraatomic LMM Auger transition, (b) and (c) two kinds of interatomic Auger transitions. The open circles indicate electron vacancies, and the cross-hatched circles indicate electrons which are quite likely removed in the initial collision and therefore may not be available to participate in the indicated transition. The relative positions of all energy levels *except* the 1s levels are drawn to scale.

in sulfur atoms of Na_2SO_4 are much more effectively screened by the surrounding environment than they are for sulfur atoms of Na_2S.

To the extent that the valence electrons in solid compounds may be considered to be totally delocalized within a region defining the molecular volume, the average valence electron density D_V may be used as a rough comparative measure of the relative valence electron transition probability. The average valence electron density of a compound is easily calculable from its mass density ρ using the equation

$$D_V = 0.602 \frac{n_V \rho}{W_{\text{mol.}}} \text{ electrons/Å}^3 , \qquad (10)$$

where n_V is the total number of valence electrons and $W_{\text{mol.}}$ is the molecular weight. The p_L values obtained for the Al, Si, S, Cl compounds are shown plotted vs D_V in Fig. 8. In all four cases the p_L values vary approximately linearly with D_V and the slope is in the expected direction. As the average valence electron density increases, the valence electron transition probability increases thereby causing p_L to decrease. The silicon results exhibit a particularly good correlation with remarkably few deviations from the straight line which has been fit through the data points. The sulfur results also correlate well with D_V except for CdS and FeS. It is interesting to note that the p_L values for the three transition element compounds CdS, ZnS, and FeS are nearly the same. Of course, the concept of "valence" is considerably less well defined for these compounds since "inner" shell as well as "outer" shell electrons are involved in the bonding. We have calculated D_V for CdS, ZnS, and FeS by somewhat arbitrarily taking the two 4s electrons in Fe and Zn and the two 5s electrons in Cd to be the valence electrons. In the case of chlorine, several compounds—most notably CsCl, KCl, and $CaCl_2$—deviate considerably from the line established by the rest of the data points. The deviations of these particular compounds are hard to account for in view of the rather good agreement displayed by compounds which are chemically quite similar, such as RbCl, NaCl, and $SrCl_2$, respectively. The most noteworthy feature of the aluminum data is the extremely small amount by which the p_L values change over a wide range of D_V. A previous suggestion that the p_L value for Al might be reduced due to the high mobility of its conduction electrons[12] is not supported by the results presented here.

It was noted earlier in a very qualitative way for several silicon and sulfur compounds that the lowest p_L values appear to occur for those compounds which are expected to have the lowest densities of valence electrons localized about the target atoms. This can be shown to be true in

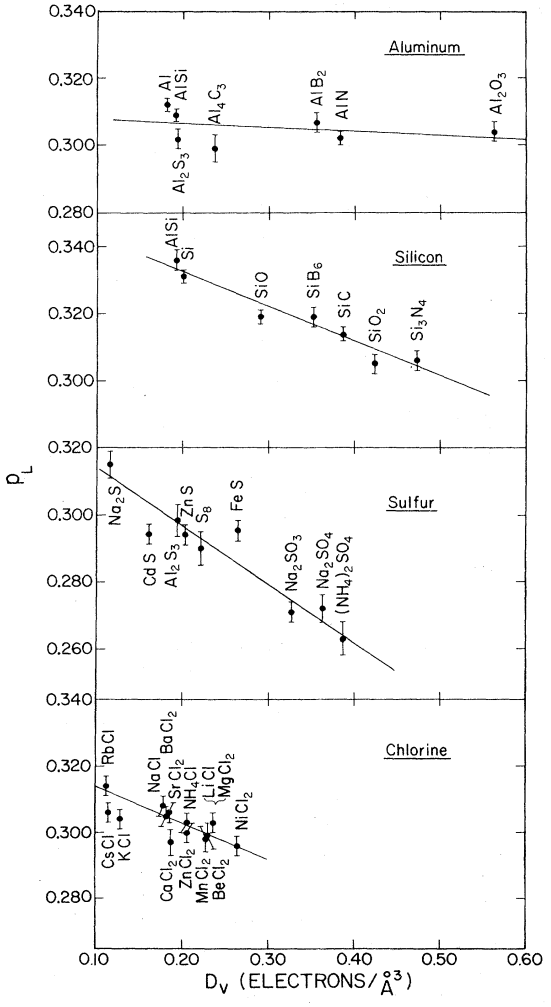

FIG. 8. Variation of p_L with average valence electron density for all of the compounds examined.

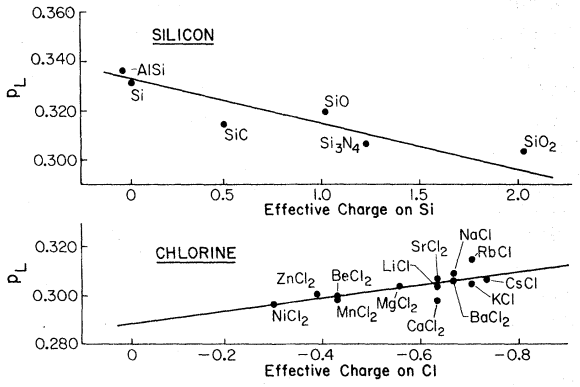

FIG. 9. Variation of p_L with effective charge for simple compounds of silicon and chlorine.

general for all of the elements studied by invoking the concept of effective charge. In a very simple treatment of effective charge one regards the oxidation number to be the number of electrons transferred in a totally ionic bond. The effective charge is then taken to be the product of the oxidation number and the bond ionicity, which as defined by Pauling[25] is given by

$$I = 1 - e^{-0.25\Delta^2},$$

where Δ is the electronegativity difference between the two atoms involved. Shown in Fig. 9 are graphs of p_L vs effective charge for those silicon and chlorine compounds to which the above definition of effective charge may reasonably be expected to apply. In both cases it is seen that p_L decreases with increasing effective (positive) charge. The p_L values for the aluminum and sulfur compounds follow this same trend.

The above observations suggest that essentially all of the valence electrons which happen to be localized about the target atom at the time of a collision are ionized. Then only the valence electrons which usually reside near the neighboring atoms are available to neutralize the tremendous center of charge produced in the vicinity of the target atom as a result of the instantaneous ejection of three or four inner-shell electrons and numerous outer-shell electrons. The more positive the target atom effective charge, the less time the valence electrons spend near the target atom and hence the less likely it is that they will be ionized in the collision. Therefore, the more the valence electron density is displaced toward neighboring atoms (before the collision), the more valence electrons there will be to participate in K- and L-vacancy filling transitions following the collision.

VI. CONCLUSIONS

The results of the present investigations have shown that chemical effects on $K\alpha$ x-ray satellite intensities are observable in a large variety of compounds of third-row elements. These effects appear to be independent of projectile atomic number, at least in the energy range around 2 MeV/amu. The fact that a definite correlation exists between p_L and average valence electron density strongly supports the conclusion that interatomic processes must contribute to the deexcitation of multiply-ionized states following heavy-ion collisions. It is clear that a great deal more information on K- and L-vacancy transfer rates in solids must be obtained before any really fundamental understanding of the factors which give rise to the dependence of $K\alpha$ x-ray satellite intensities on chemical environment can be reached.

ACKNOWLEDGMENTS

We wish to thank Jack Demarest, Mark Michael, and Jeffrey Sjurseth for their help with the experiments, and Joaquin Hernandez for making the evaporated targets. Credit is due to M. K. Bahl for pointing out the applicability of effective charge to our measurements. The assistance of Edwin Peeler, Wilmer Walterscheid, Shirley Dean, and the rest of the cyclotron staff is gratefully acknowledged.

---

*Work supported in part by the Robert A. Welch Foundation and the U. S. Energy Research and Development Administration.

[1]For a recent review of this subject see P. Richard in *Atomic Inner-Shell Processes*, edited by B. Crasemann (Academic, New York, 1975), Vol. I, p. 73.
[2]D. Burch and P. Richard, Phys. Rev. Lett. 25, 983 (1970).
[3]A. R. Knudson, D. J. Nagel, P. G. Burkhalter, and K. L. Dunning, Phys. Rev. Lett. 26, 1149 (1971).
[4]D. Burch, P. Richard, and R. L. Blake, Phys. Rev. Lett. 26, 1355 (1971).
[5]T. K. Li, R. L. Watson, and J. S. Hansen, Phys. Rev. A 8, 1258 (1973).
[6]R. L. Watson, F. E. Jenson, and T. Chiao, Phys. Rev. A 10, 1230 (1974).
[7]C. P. Bhalla, Phys. Rev. A 12, 122 (1975).
[8]F. P. Larkins, J. Phys. B 4, L29 (1971).
[9]P. Richard, J. Bolger, D. K. Olsen, and C. F. Moore, Phys. Lett. 41A, 269 (1972).
[10]P. G. Burkhalter, A. R. Knudson, D. J. Nagel, and K. L. Dunning, Phys. Rev. A 6, 2093 (1972).
[11]J. McWherter, D. K. Olsen, H. H. Wolter, and C. F. Moore, Phys. Rev. A 10, 200 (1974).
[12]R. L. Watson, T. Chiao, and F. E. Jenson, Phys. Rev. Lett. 35, 254 (1975).
[13]R. L. Watson, T. Chiao, F. E. Jenson, and B. I. Sonobe, in *Beam-Foil Spectroscopy*, edited by I. A. Sellin and D. J. Pegg (Plenum, New York, 1976), Vol. 2, p. 567.
[14]R. L. Kauffman, J. H. McGuire, P. Richard, and C. F. Moore, Phys. Rev. A 8, 1233 (1973).
[15]J. D. Garcia, Phys. Rev. A 1, 280 (1970).
[16]L. C. Northcliffe and R. F. Schilling, Nucl. Data Tables A 7, 233 (1970).
[17]E. Storm and H. I. Israel, Nucl. Data Tables A 7, 565 (1970).
[18]B. I. Sonobe and R. L. Watson (unpublished).
[19]T. L. Hardt, Ph.D. thesis, Texas A&M University, 1975 (unpublished).
[20]A. R. Knudson, P. G. Burkhalter, and D. J. Nagel, in Proceedings of the Fifth International Conference on Atomic Collisions, Gatlinburg, 1973 (unpublished).

[21]J. P. Desclaux, At. Data Nucl. Data Tables 12, 311 (1973).
[22]J. Valasek, Phys. Rev. 53, 274 (1938).
[23]T. Åberg, in Proceedings of the International Symposium on X-Ray Spectra and Electronic Structure of Matter, Munich, 1972 (unpublished).
[24]P. H. Citrin, J. Electron. Spectrosc. Relat. Phen. 5, 273 (1974).
[25]L. Pauling, *The Nature of the Chemical Bond* (Cornell U.P., Ithaca, N.Y., 1960).